Measuring Observer Metamerism: The Nimeroff Approach

Mark D. Fairchild, Rodney L. Heckaman*

Munsell Color Science Laboratory, Coloege of Science, Rochester Institute of Technology, 54 Lomb Memorial Drive, Rochester, New York 14623

Received 7 May 2014; revised 23 January 2015; accepted 23 January 2015

Abstract: In a color matching experiment, the colors of two stimuli might match perfectly to one observer. However, to another, those same two stimuli might not match depending on the spectral characteristics of the two stimuli and each of the observers' visual responses. This phenomenon, that any two observers perceive color matches differently, is termed observer metamerism. Only recently have differences in the factors that affect the spectral response of the human eye been quantified to a degree such that observer metamerism can be realistically modeled over a representative population of human observers. From the statistics of these factors, a large, representative group of such observers—each said to be metameric to a standard—was created in terms of LMS cone spectral responses. Using analysis of variance and error propagation, as suggested by Nimeroff, this sample set was reduced to a complete colorimetric description that includes mean color matching functions along with variance and covariance functions. This simplified representation is then applied to creating arbitrary sets of color matching functions, such as the CIE 1931 and 1964 observers, and their covariance functions to allow the practical characterization of observer-metameric mismatch gamuts for any nominally metameric stimulus pair. © 2015 Wiley Periodicals, Inc. Col Res Appl, 00, 000–000, 2015; Published Online 00 Month 2015 in Wiley Online Library (wileyonlinelibrary.com). DOI 10.1002/col.21954

Key words: observer; metamerism; color perception

INTRODUCTION

In a color matching experiment, the colors of two objects might match perfectly to one observer; yet to another, those same two objects might not match depending on the spectral characteristics of the stimuli and each of the observers' eye responses. This phenomenon that no two observers perceive color the same is termed observer metamerism. In order to characterize fully this phenomenon, Nimeroff *et al.*[1] presented what they considered a fundamental procedure for describing "a complete standard observer system [that] should contain not only the mean spectral tristimulus functions derived from the color-mixture data, but should contain, also, the variances and covariances of these functions as derived from the within- and between-observer [variability] of the color-mixture data." From this description, "the extent to which a normal observer tends to make different matches on successive attempts, and the extent to which different normal observers vary one from another" can be quantified.

Up until just recently, there was no way to measure this variability reliably over a large enough sample representative of the human population. Instead, in 1931, the CIE characterized a standard observer in the form of three color matching functions that form the basis of the measurement of color[2] and a much later standard deviate observer in 1989.[3] It should be noted, of course, that measurements and analyses of dispersion in the original color matching data for the CIE standard observers were made by Wyszecki and Stiles.[4] More recently, in a article on the molecular genetics of color vision, Neitz and Neitz[5] summarized their work and the works of in vitro experiments of Merbs and Nathans[6] and Asenjo *et al.*[7] that determined the effect of certain amino acid substitutions along the X chromosome strand on the spectral tuning of the L and M photopigments apparently discretely shifting their peak spectral response. These results are shown in Fig. 1 illustrating the widely accepted discrete (and possibly multimodal or bimodal) nature of their respective relative responses.

However, the results of Sharpe and Stockman[8–10] show that both L and M cone peak wavelengths, when considered as part of a full eye, have a more continuous range

*Correspondence to: Rodney L. Heckaman (e-mail: rlh9572@cis.rit.edu)

Additional Supporting Information may be found in the online version of this article.

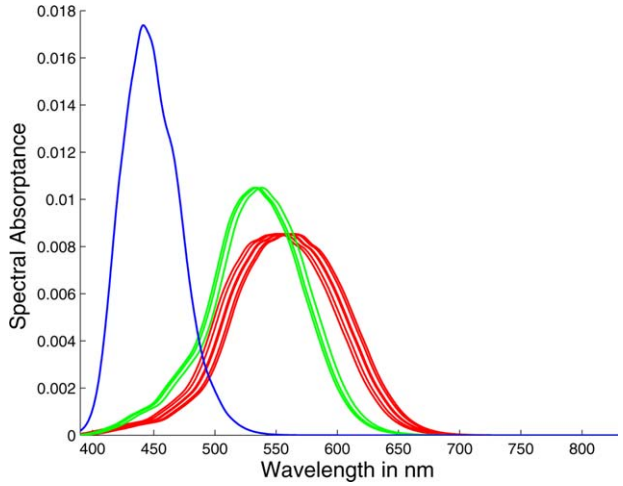

Fig. 1. Discrete L (red), M (green), and S (blue) photopigment absorption by genotype from Neitz and Neitz[5] normalized to equal area.

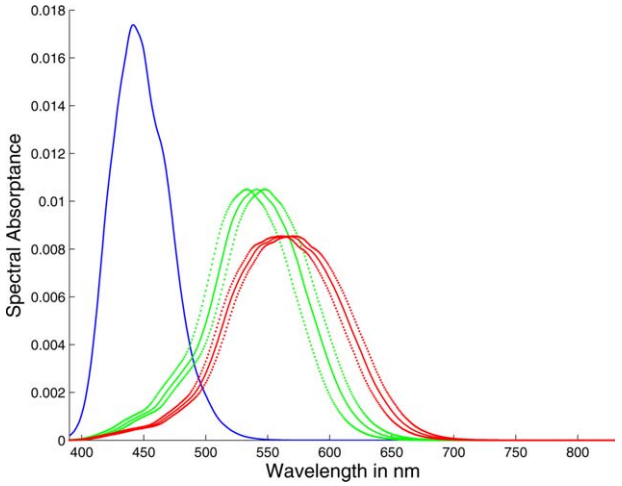

Fig. 2. The LMS photopigment absorption from Sharpe and Stockman[8–10] normalized to equal area. The mean functions used in the computational model are shown together with plus-and-minus three-sigma curves.

of variation due to differences in ocular media transmittance, cone shape, and pigment density. Thus, continuous unimodal distributions of cone peak wavelength are used in the present models. It is possible that further advances in measurement precision and volume will allow such a model to be refined to a multimodal or bimodal distribution in peak wavelength of the L, and perhaps M, cones. Their baseline cone spectral response functions (sometimes called cone fundamentals) were then derived as illustrated in Fig. 2. From these results, the CIE Technical Committee 1-36 of Division 1, Vision and Color, published a report in 2006[11] on their estimates of the cone fundamentals for an average normal observer as a function of age and field size with corrections for the aging of the lens and the density of the macula (Fig. 3). The CIE 2006 functions, however, do not address individual variations in color matching (only changes in the mean functions with age and field size). Further relevant analyses of variation in color vision and color matching have been completed by Webster and MacLeod[12] and Viénot.[13]

COMPUTATIONAL MODEL OF COLOR MATCHING FUNCTIONS

The color matching experiment used here to derive estimates of color matching functions with monochromatic primaries can be characterized as a system of three linear equations with three unknowns at each wavelength given that a unit of energy of wavelength, $\angle$, is matched by RGB amounts of three monochromatic primaries of unit energy at wavelengths $\angle_R$, $\angle_G$, and $\angle_B$. Equation (1) defines this system where T_l and T_m, are the spectral transmittances of the lens and macula respectively, L, M, and S, are the cone photopigment absorption functions, and R, G, and B, are the spectral tristimulus values.[14] Solving Eq. (1) for R, G, and B at each wavelength results in the determination of a set of color-matching functions for the $\angle_R$, $\angle_G$, and $\angle_B$ monochromatic primaries.

$$\begin{vmatrix} T_l(\lambda)T_m(\lambda)L(\lambda) \\ T_l(\lambda)T_m(\lambda)M(\lambda) \\ T_l(\lambda)T_m(\lambda)S(\lambda) \end{vmatrix} = \begin{vmatrix} R(\lambda)T_l(\lambda_R)T_m(\lambda_R)L(\lambda_R)+G(\lambda)T_l(\lambda_G)T_m(\lambda_G)L(\lambda_G)+B(\lambda)T_l(\lambda_B)T_m(\lambda_B)L(\lambda_B) \\ R(\lambda)T_l(\lambda_R)T_m(\lambda_R)M(\lambda_R)+G(\lambda)T_l(\lambda_G)T_m(\lambda_G)M(\lambda_G)+B(\lambda)T_l(\lambda_B)T_m(\lambda_B)M(\lambda_B) \\ R(\lambda)T_l(\lambda_R)T_m(\lambda_R)S(\lambda_R)+G(\lambda)T_l(\lambda_G)T_m(\lambda_G)S(\lambda_G)+B(\lambda)T_l(\lambda_B)T_m(\lambda_B)S(\lambda_B) \end{vmatrix} \quad (1)$$

Lens Spectral Transmittance

The lens spectral transmittance function in the color matching function simulation is derived from the two-component model of Pokorny and Smith.[15–17] According to the two-component model, the lens spectral transmittance is made up of one component, *TL2*, that remains stable after age 20 and a second component, *TL1*, affected by aging. Average lens transmittance functions are then computed as a function of observer age, A, using Eq. (2) for observers between the ages of 20 and 60 years and Eq. (3) for observers older than 60 years.

$$T_l = T_{L1}[1+0.02(A-32)]+T_{L2} \quad (2)$$

$$T_l = T_{L1}[1.56+0.0667(A-60)]+T_{L2} \quad (3)$$

To represent a population of observers for a Monte Carlo simulation of color matching functions, the observer age, A, was randomly selected according to the

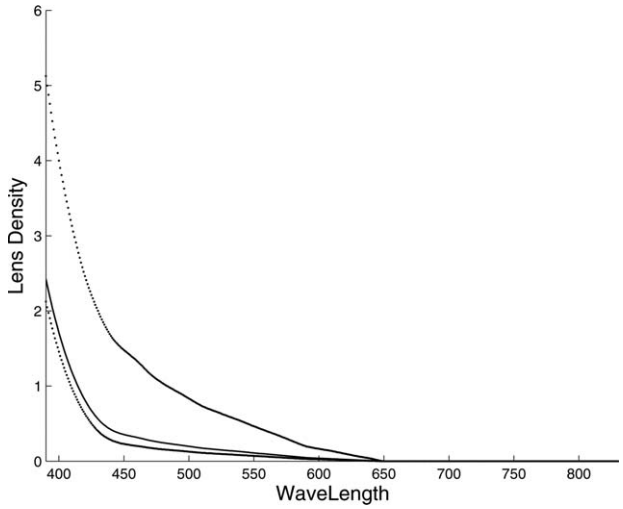

Fig. 3. The individual, mean lens transmittance according to Pokorny and Smith[16] with plus-and-minus three sigma functions from the computational model.

probability density function defined by the histogram of ages in the population of the United States during the 2000 census (Fig. 4).

In addition to this age dependence, the lens transmittance has random variation between observers of identical age that Pokorny and coworkers[15–17] characterized in terms of a variation in the age predicted by the model for observers of a given age. This variability, expressed in terms of age in the two-component model was found to have a standard deviation of 20% of the actual age. This added variability is represented in the Monte Carlo color matching function model by first selecting an observer age randomly from the census-data distribution, and then randomly perturbing that age according to Eq. (4).

$$A = A_{cencus} + \delta \tag{4}$$

A is the age ultimately used for a random individual observer in the simulation, A_{census} is the age initially selected from the census-data distribution (limited to the

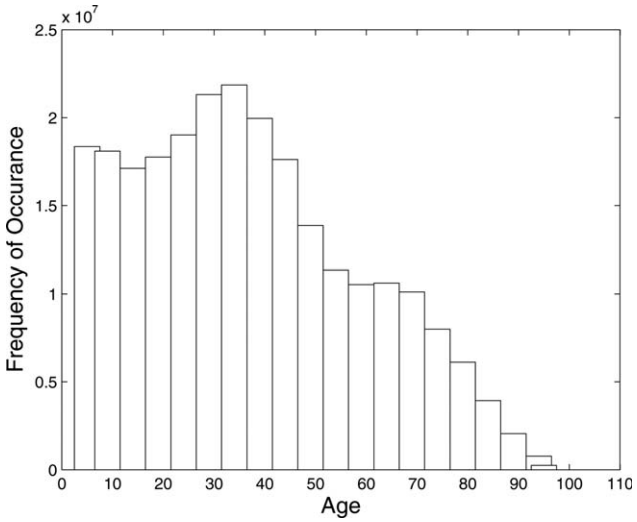

Fig. 4. Age distribution in the population of the United States during the 2000 census.

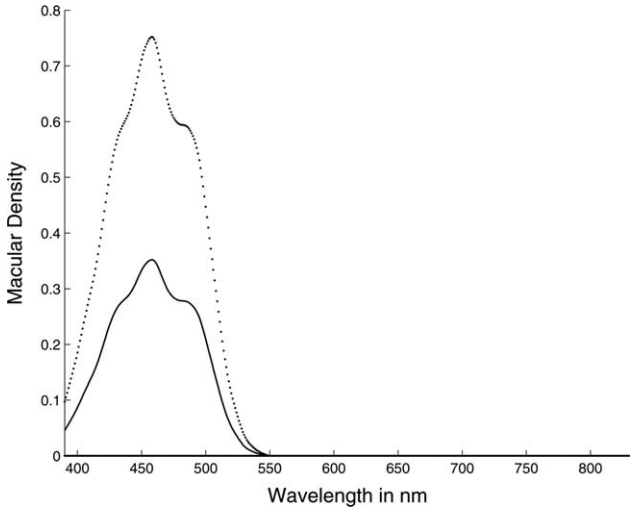

Fig. 5. The individual, mean macular density function, $D_{m,Bone}$ from Bone *et al.*[18] along with plus-and-minus three sigma functions from the computational model. Note that the minus three sigma function is effectively zero density across all wavelengths.

range from 20-75 years), and ^{TM} is a normally-distributed random variable with a mean of 0.0 and standard deviation of $0.20A_{\text{census}}$. The sampled result, shown in Fig. 5, is essentially to low-pass filter the census data histogram.

Macula Spectral Transmittance

The macula is an ovate, yellow pigmented area covering the fovea that subtends $\sim 2^\circ$ where observers fixate objects of interest. It should be noted that the macular density is nonhomogenous across this region and varies significantly from observer to observer. It protects the fovea against the harmful effects of sunlight. The baseline macular pigment spectral density (converted to transmittance for the simulation of color matching functions) function used is that of Bone *et al.*[18] These data are similar to others that have been published and described by Berendschot and van Norren.[19]

Berendschot and van Norren estimate that the standard deviation of peak macular density is 0.13. This value along with a normal probability distribution was used in the Monte Carlo simulation. It was assumed that the variability across observers is multiplicative in density in order to preserve zero density values for all observers at the wavelengths where the macular pigment does not absorb light. The Bone *et al.* data[17] have a peak macular density of 0.352. Thus, Eq. (5) was used to scale the baseline macular function randomly to represent various individual observers.

$$D_m(\lambda) = D_{m,Bone}(\lambda)\left\lfloor \frac{0.352+\delta}{0.352} \right\rfloor \tag{5}$$

D_{m} is the individual macular density function, $D_{\text{m,Bone}}$ is the average function of Bone *et al.*[17] illustrated in Fig. 5, and ^{TM} is a normally distributed random variable with a mean of 0.0 and standard deviation of 0.13. Van de

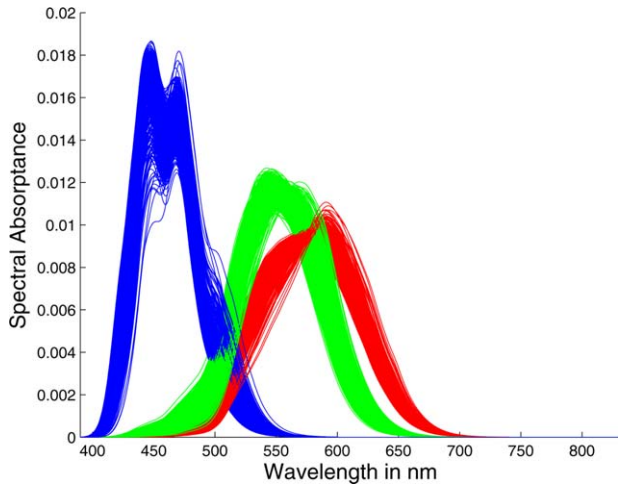

Fig. 6. One thousand LMS photopigment absorption functions representative of the human population and normalized to equal area.

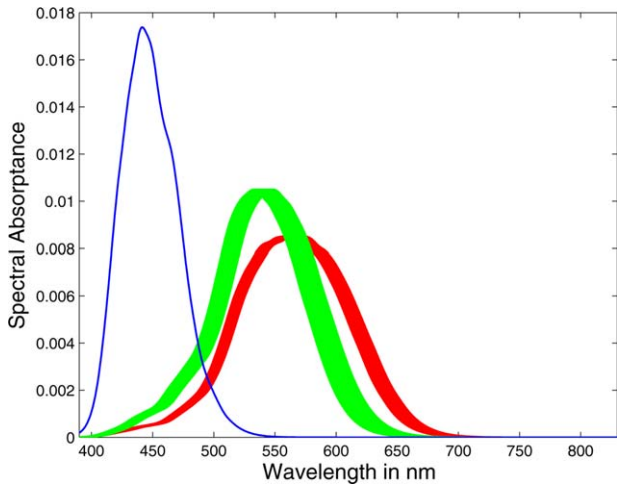

Fig. 7. One thousand LMS cone fundamentals representative of the human population normalized to equal area.

Kraats *et al.*[20] have described a two-component model of macular pigment density that might suggest a more complex model of variance in the macula could be derived. For the purpose of this work, the single-component, multiplicative in density, model appears adequate.

LMS Cone Photopigment Absorptance

The variability in cone spectral absorption across observers has been studied recently through both genetic and psychophysical techniques.[8–10] In these studies, the L and M photographic pigment absorption functions are summarized in a population of observers as a statistical, normal distribution of peak wavelengths with the L cones having a standard deviation of 1.6 nm and the M-cones a standard deviation of 2.5 nm. Note that this assumes unimodal distributions of cone peak sensitivity that are not supported by the genetic suggestion of discrete cone variations. However, this is the best, and most effective model currently available given experimental uncertainty and other variations in cone responsivity such as pigment density. Improved models of cone photopigment statistics might well be generated in the future. The S-cone response is taken to have no variability between observers since any variability will be small compared to the variability caused by the lens and macula transmittance functions. Again, improved data might allow future refinement of this S-cone model. These standard deviation estimates come directly from the data of Sharpe *et al.*[8] and are slightly different from some other suggestions. It is almost certain that more accurate estimates can and will be made in the future.

The L and M photopigment absorption functions were randomly selected by transforming the baseline photopigment absorption functions from wavelength (nm) to wave-number (cm^{-1}) then shifting the baseline additively so that their peak wavelength coincides with the respective sampled, peak wavelength. This wave-number representation is consistent with the work of Dartnall[21] and Wyszecki and Stiles[4] illustrating that absorption curves typically retain their shape across changes in peak wavelength when represented on a wave-number scale. Others have illustrated that the shift of spectral absorption curves along the wave number axis might not preserve curve shape for visual pigments.[22,23] However the shifts utilized in this computational model are quite small, so any discrepancies would be small enough to not impact the final results. The resulting LMS photopigment absorption for each of 1,000 randomly selected observers is illustrated in Fig. 6.

LMS Cone Fundamentals

The S, M, and L cone fundamentals are then computed via Eq. (1) for 1000 simulated individuals randomly sampled from those statistics of cone photopigment absorption, macula density, and lens aging that affect the spectral response of the human eye. Observer metamerism is then quantified over a representative population of human observers using Monte Carlo analysis techniques.

Figure 7 illustrates these LMS cone fundamentals shown as blue, green, and red respectively. The dual peaks observed in these functions are due to the normalization to equal area and the shifting values of ocular media density. No single function has dual peaks (beyond the small "shoulder" sometimes observed in the short-wavelength functions due to the features of the macular pigment density). It should also be noted that overlapping plots of 1000 functions can be misleading because a few extreme functions are visually represented in the same manner as the majority of functions near the mean. It should be carefully noted that the dual peaks are not due to so-called beta-band absorptions in the cone photopigments, which are much less significant and at much more discrepant wavelengths.

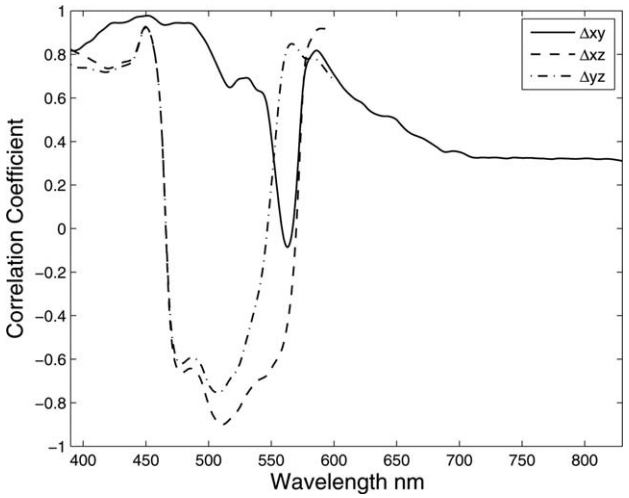

Fig. 8. Mean LMS cone fundamental spectral absorption (solid lines) normalized to a peak absorptance of unity and the square root of their variance (dotted lines).

THE NIMEROFF APPROACH AND THE ANALYSIS OF VARIANCE

Now, having the LMS cone fundamentals for a representative population of individuals derived as in the above, it is now possible to describe Nimeroff's complete standard observer that includes the between-observer covariance Σ_{LMS} across the 1,000 observers given by[1]:

$$\Sigma_{LMS}(\lambda) = \begin{vmatrix} \sigma_L^2(\lambda) & \sigma_{LM}(\lambda) & \sigma_{LS}(\lambda) \\ \sigma_{ML}(\lambda) & \sigma_M^2(\lambda) & \sigma_{MS}(\lambda) \\ \sigma_{SL}(\lambda) & \sigma_{SM}(\lambda) & \sigma_S^2(\lambda) \end{vmatrix} \tag{6}$$

for $\sigma_i^2(\lambda)$ the variance in L, M, S, and $\sigma_{ij}(\lambda)$ the covariance between LMS cone fundamentals at each wavelength λ across the 1000 representative observers. Figure 8 illustrates the mean spectral absorptance of the LMS cone fundamentals averaged across the observers normalized to their respective peak values and the square root of their respective variances in 1 nm increments of wavelength. The LMS covariance matrix is given in Appendix A (available in the Supporting Material online) in 5 nm increments of wavelength.

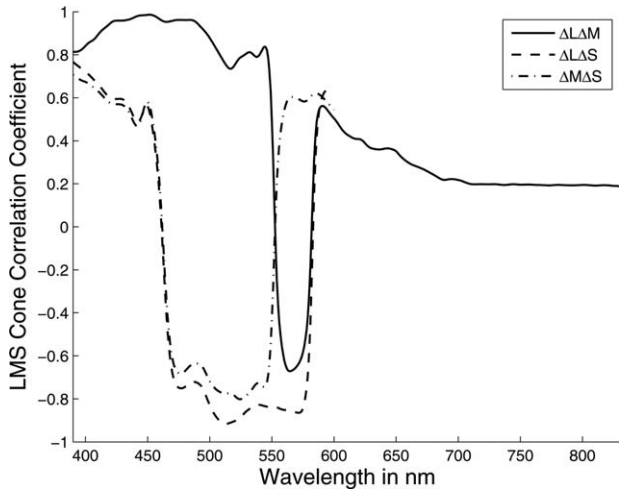

Fig. 9. LMS cone spectral correlation coefficients.

Figure 9 illustrates their respective correlation coefficients ρ_{ij} that relates the covariance $\sigma_{ij}(\lambda)$ to the variances $\sigma_i^2(\lambda)$ and $\sigma_j^2(\lambda)$ given by:

$$\rho_{ij}(\lambda) = \frac{\sigma_{ij}(\lambda)}{\sqrt{\sigma_i^2(\lambda)\sigma_j^2(\lambda)}} \tag{7}$$

According to Burns and Berns,[24] "[the] fact that the three [LMS cone responses] overlap at various wavelengths introduces correlation into the error ..." as illustrated. And furthermore, according to Nimeroff, *et al.*,[1] "... a positive correlation coefficient implies that if an observer uses more (or less) than average of one instrumental primary in making a match, he uses more (or less), respectively, than average of the other primary, also. Conversely, a negative correlation coefficient implies that if more (or less) than average of one primary is used, less (or more), respectively, than average of the other primary is used."

Propagation to Color Matching Functions

Since any arbitrary set of color matching functions $\Psi_{\lambda,x}, \Psi_{\lambda,y}, \Psi_{\lambda,z}$ analogous to the CIE system can be expressed as a linear combination of the LMS cone fundamentals, Nimeroff's complete description of the standard observer in terms of the LMS cone fundamentals can be extended to a set of arbitrary color matching functions by the following.

$$\bar{\Psi} = \begin{vmatrix} \bar{\Psi}_{\lambda,x} \\ \bar{\Psi}_{\lambda,x} \\ \bar{\Psi}_{\lambda,x} \end{vmatrix}_{2^\circ} = \begin{vmatrix} k_1 & k_2 & k_3 \\ k_4 & k_5 & k_6 \\ k_7 & k_8 & k_9 \end{vmatrix} \begin{vmatrix} \bar{L}_\lambda \\ \bar{M}_\lambda \\ \bar{S}_\lambda \end{vmatrix} = KX \tag{8}$$

for $\bar{\Psi}$ the mean color matching function of the representative population of observers, and $X = |\bar{L}_\lambda \quad \bar{M}_\lambda \quad \bar{S}_\lambda|^T$, and their mean LMS cone. Solving using an estimated least squares fit to the CIE 1931 Standard Colorimetric Observer gives:

$$K = \bar{\Psi}\, X^T (XX^T)^{-1} \tag{9}$$

where X^T denoting the transpose of the vector X.

For the purpose of this analysis, within-observer variability is assumed the same across all the observers. Hence, the between observer covariance matrix Σ_{xyz} given by:

$$\Sigma_{xyz}(\lambda) = \begin{vmatrix} \sigma_x^2(\lambda) & \sigma_{xy}(\lambda) & \sigma_{xz}(\lambda) \\ \sigma_{yx}(\lambda) & \sigma_y^2(\lambda) & \sigma_{ys}(\lambda) \\ \sigma_{zx}(\lambda) & \sigma_{zy}(\lambda) & \sigma_z^2(\lambda) \end{vmatrix} \tag{10}$$

where, omitting the λ notation, the variances are given by Nimeroff[1] as:

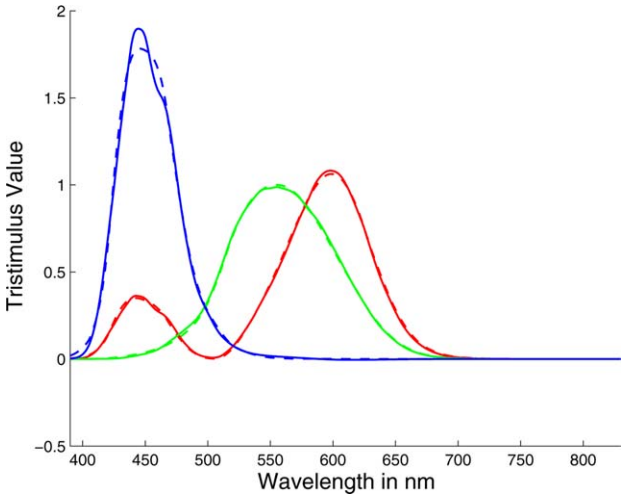

Fig. 10. Estimated 2° observer (solid line) and CIE 1931 2° observer (dotted line) spectral tristimulus values.

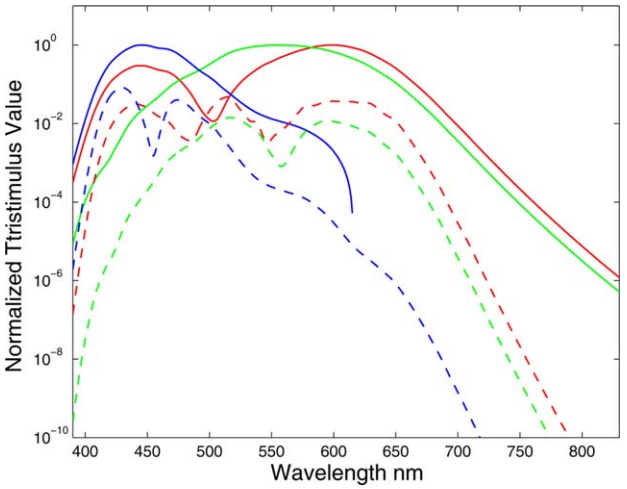

Fig. 11. Mean spectral tristimulus values for the estimated 2° observers normalized to a peak value of unity (solid lines) and their square-root variances (dotted lines).

$$\begin{aligned}
\sigma_x^2 &= k_1^2\sigma_L^2+k_2^2\sigma_M^2+k_3^2\sigma_S^2+2(k_1k_2\sigma_{LM}+k_1k_3\sigma_{LS}+k_2k_3\sigma_{MS})\\
\sigma_y^2 &= k_4^2\sigma_L^2+k_5^2\sigma_M^2+k_6^2\sigma_S^2+2(k_4k_5\sigma_{LM}+k_4k_6\sigma_{LS}+k_5k_6\sigma_{MS})\\
\sigma_z^2 &= k_7^2\sigma_L^2+k_8^2\sigma_M^2+k_9^2\sigma_S^2+2(k_7k_8\sigma_{LM}+k_7k_9\sigma_{LS}+k_8k_9\sigma_{MS})
\end{aligned} \tag{11}$$

and the covariances as:

$$\begin{aligned}
\sigma_{xy} &= k_1k_4\sigma_L^2+k_2k_5\sigma_M^2+k_3k_6\sigma_S^2+(k_1k_5+k_2k_4)\\
&\quad \sigma_{LM}+(k_1k_6+k_3k_4)\sigma_{LS}+(k_2k_6+k_3k_6)\sigma_{MS}\\
\sigma_{xz} &= k_1k_7\sigma_L^2+k_2k_8\sigma_M^2+k_3k_9\sigma_S^2+(k_1k_8+k_2k_7)\\
&\quad \sigma_{LM}+(k_1k_9+k_3k_7)\sigma_{LS}+(k_2k_9+k_3k_8)\sigma_{MS}\\
\sigma_{xz} &= k_4k_7\sigma_L^2+k_5k_8\sigma_M^2+k_6k_9\sigma_S^2+(k_4k_8+k_5k_7)\\
&\quad \sigma_{LM}+(k_4k_9+k_6k_7)\sigma_{LS}+(k_5k_9+k_8k_8)\sigma_{MS}
\end{aligned} \tag{12}$$

APPLICATION OF THE NIMEROFF APPROACH: THE CIE 1931 AND 1964 OBSERVER

Solving for K in Eq. (9) for the CIE 1931 2° Observer color matching functions $\bar{x}_\lambda, \bar{y}_\lambda, \bar{z}_\lambda$ gives:

$$K = \begin{vmatrix} 1.7457 & -1.1476 & 0.3367 \\ 0.4347 & 0.6461 & 0.0411 \\ 0.0693 & -0.1125 & 1.8550 \end{vmatrix}$$

The estimated mean 2° standard observer is plotted in Fig. 10 against the CIE 1931 2° Observer.

The covariance matrix Σ_{xyz} can then be obtained from Eqs. (10)–(12). Figure 11 illustrates the estimated mean 2° Observer spectral tristimulus values $\hat{x}_\lambda, \hat{y}_\lambda, \hat{z}_\lambda$ from Eq. (8) and the square root of their respective variances from Eq. (10), and Fig. 12 illustrates their respective correlation coefficients given by Eq. (7) in 1 nm increments of wavelength. The CIE XYZ covariance matrix is given in Appendix B (available in the Supporting Material online) in 5 nm increments of wavelength.

In the same manner as in Eq. (9), an approximation to the CIE 1964 10° Observer color matching functions $\bar{x}_\lambda$, $\bar{y}_\lambda, \bar{z}_\lambda$ can be computed as a linear combination of the mean LMS cone fundamentals $\bar{L}_\lambda, \bar{M}_\lambda, \bar{S}_\lambda$, of the sampled representative population of cone fundamentals as given below and illustrated in Fig. 13.

$$K = \begin{vmatrix} 1.7749 & -1.07386 & 0.3537 \\ 0.4362 & 0.6706 & 0.1374 \\ 0.1063 & -0.1747 & 2.0154 \end{vmatrix}$$

The corresponding covariance matrix can then be computed according to Eqs. (10)–(12). The CIE 10 XYZ covariance matrix is given in Appendix C (available in the Supporting Material online) in 5 nm increments of wavelength. Note that the fit to the CIE 10° observer functions is not as good as the fit to the CIE 2° observer

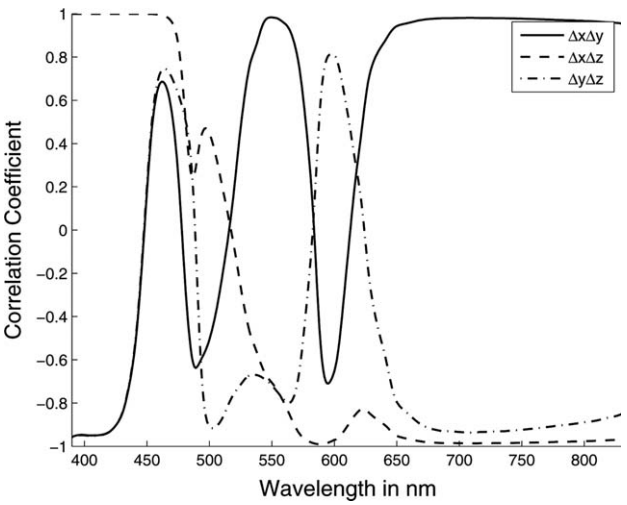

Fig. 12. Correlation coefficients for the CIE 1931 color matching functions.

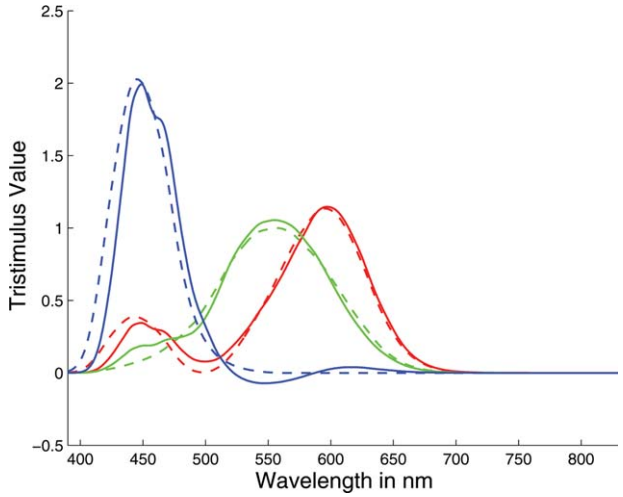

Fig. 13. Estimated 10° observer (solid line) and CIE 1964 observer (dotted line) spectral tristimulus values.

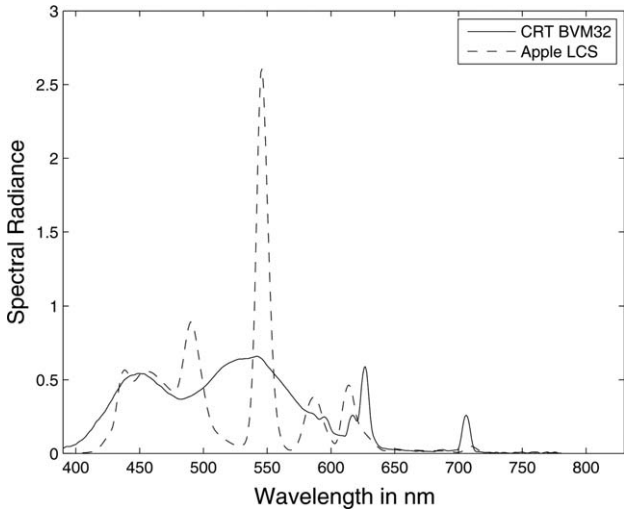

Fig. 14. Spectral radiance of Patch 6, bluish green, of the X-Rite Color Checker Chart rendered to two displays, an Sony BVM32 CRT display (solid line) and an Apple, LED backlit, LCD display (dotted line), such that they match for the CIE 1931 2° Observer.

functions. This is because the computational model was derived and implemented for small-field properties of color matching (e.g., 2° cone fundamentals, presence of macular pigment). To make a more proper estimate of the variation in color matching for large fields, the computational model would need to be modified to include field sized dependency as in the CIE 2006 model.[11] For the moment, simply applying the same covariance functions, linearly transformed, to various mean color matching functions is adequate and a huge improvement over the current state of affairs of using no covariance functions at all.

PRACTICAL APPLICATION: THE MATCH/NO MATCH CONDITION

As an illustration of an application of the covariance matrix representation, a number of patches from the X-Rite Color Checker Chart were rendered to two displays, a Sony BVM32, CRT, broadband display and an Apple, LED backlit, LCD, narrowband display. The pairs were rendered to match for the CIE 1931 standard observer. Then, solely from the covariance matrix derived for the CIE 1931 Observer and the differences in the spectra of the rendered pair, a procedure is derived and applied to quantify and draw the 95th percentile ellipsoid in the degree of miss-match in CIELAB across the representative population of observers when comparing two displays of differing spectral radiance properties.

Rendering

For the CIE XYZ values of a patch and each display with respective primaries $|P(\lambda)_r \quad P(\lambda)_g \quad P(\lambda)_b|_{\text{Sony}}$ and $|P(\lambda)_r \quad P(\lambda)_g \quad P(\lambda)_b|_{\text{Apple}}$, the patch is rendered as stimulus S:

$$S(\lambda) = c_r P_r(\lambda) + c_g P_g(\lambda) + c_b P_b(\lambda) \tag{13}$$

with concentrations of each primary $C = |c_r \quad c_g \quad c_b|^T$ given by:

$$C = M^{-1} XYZ \tag{14a}$$

where:

$$M = m * diag(L) \tag{14b}$$

$$L = m^{-1} \begin{vmatrix} \frac{Xn}{Yn} & 1 & \frac{Zn}{Yn} \end{vmatrix} \tag{14c}$$

for $XYZ_n = |95.047 \quad 100.000 \quad 108.883|$ the CIE D65 white point tristimulus values:

$$m = \begin{vmatrix} \frac{R_X}{R_Y} & \frac{G_X}{G_Y} & \frac{B_X}{B_Y} \\ 1 & 1 & 1 \\ \frac{R_z}{R_Y} & \frac{G_z}{G_Y} & \frac{B_z}{B_Y} \end{vmatrix} \tag{14d}$$

and for R, G, and B the tristimulus values of each primary given by:

$$R = \frac{R}{R_x + R_Y + R_Z} \quad G = \frac{G}{G_x + G_Y + G_Z} \quad B = \frac{B}{B_x + B_Y + B_Z}$$

$$R = |R_x \ R_Y \ R_Z|' = k \sum\nolimits_{\lambda} |\bar{x}(\lambda) \quad \bar{y}(\lambda) \quad \bar{z}(\lambda)|_{2^\circ}' P_r(\lambda) \Delta\lambda \tag{14e}$$

$$G = |G_x \ G_Y \ G_Z|' = k \sum\nolimits_{\lambda} |\bar{x}(\lambda) \quad \bar{y}(\lambda) \quad \bar{z}(\lambda)|_{2^\circ}' P_g(\lambda) \Delta\lambda \tag{14f}$$

$$B = |B_x \ B_Y \ B_Z|' = k \sum\nolimits_{\lambda} |\bar{x}(\lambda) \quad \bar{y}(\lambda) \quad \bar{z}(\lambda)|_{2^\circ}' P_b(\lambda) \Delta\lambda \tag{14g}$$

$$\tag{14h}$$

where $\Delta\lambda$ is the wavelength interval (1 nm), $|\bar{x} \quad \bar{y} \quad \bar{z}|_{2^\circ}'$ the CMFs for the CIE 1931 2° Observer, and $k = 100 / \sum_{\lambda} \bar{y}(\lambda) \Delta\lambda$. Figure 14 illustrates the resulting spectral radiances for patch 6, bluish-green and each display.

Derivation of the CIE L*a*b* Covariance Matrix

From Alfvin and Fairchild,[25] a covariance matrix Σ_{XYZ} in CIE XYZ tri-stimulus values between the two stimuli can be computed from the covariance matrix Σ_{xzy} for the set of CMFs in *XYZ* primaries of representative observers obtained from Eqs. (10)–(12) according to:

$$\begin{aligned}&|\sigma_X^2(\lambda)\ \ \sigma_Y^2(\lambda)\ \ \sigma_Z^2(\lambda)\ \ \sigma_{XY}(\lambda)\ \ \sigma_{XZ}(\lambda)\ \ \sigma_{YZ}(\lambda)|'\\ &= \Sigma_\lambda \Delta S(\lambda)|\sigma_x^2(\lambda)\ \ \sigma_y^2(\lambda)\ \ \sigma_z^2(\lambda)\ \ \sigma_{xy}(\lambda)\ \ \sigma_{xz}(\lambda)\ \ \sigma_{yz}(\lambda)|'\Delta\lambda\end{aligned} \tag{15}$$

for $\Delta S = |S_{AppleLCS} - S_{SonyBCM32}|$ the difference in spectral radiance of the two stimuli. Then:

$$\Sigma_{XYZ}(\lambda) = \begin{vmatrix} \sigma_X^2(\lambda) & \sigma_{XY}(\lambda) & \sigma_{XZ}(\lambda) \\ \sigma_{YX}(\lambda) & \sigma_Y^2(\lambda) & \sigma_{YZ}(\lambda) \\ \sigma_{ZX}(\lambda) & \sigma_{ZY}(\lambda) & \sigma_Z^2(\lambda) \end{vmatrix} \tag{16}$$

Then, assuming spectrally uncorrelated error within each observer,[25] the effect of the overlapping color matching functions, derived in the above, on the systematic error or accuracy between metameric observers can be quantified. A correlation across wavelengths could be added to the model, but it would provide little gain in performance in exchange for a significant increase in model complexity.[25]

From Alfvin and Fairchild,[25] this systematic error as expressed by the covariance matrix in CIE L*a*b* for a color stimulus of CIE XYZ tristimulus value is given by:

$$\Sigma_{Lab}(\lambda) = M\Sigma_{XYZ}(\lambda)M' \tag{17}$$

where:

$$M = \begin{vmatrix} 0 & \frac{\delta}{\delta Y}L* & 0 \\ \frac{\delta}{\delta X}a* & \frac{\delta}{\delta Y}b* & 0 \\ 0 & \frac{\delta}{\delta Y}b* & \frac{\delta}{\delta Z}b* \end{vmatrix}$$

$$= \begin{vmatrix} 0 & \frac{116}{3Y_n}\left(\frac{Y}{Yn}\right)^{-\frac{2}{3}} & 0 \\ \frac{500}{3X_n}\left(\frac{X}{Xn}\right)^{-\frac{2}{3}} & -\frac{500}{3Y_n}\left(\frac{Y}{Yn}\right)^{-\frac{2}{3}} & 0 \\ 0 & \frac{200}{3Y_n}\left(\frac{Y}{Yn}\right)^{-\frac{2}{3}} & -\frac{200}{3Z_n}\left(\frac{Z}{Zn}\right)^{-\frac{2}{3}} \end{vmatrix} \tag{18}$$

and $XYZ_n = |95.047 \quad 100.000 \quad 108.883|$ the CIE D65 white point tristimulus values.

The 95th Percentile Solid Ellipsoid

Then, having the covariance matrix Σ_{Lab} for the differences in CIE L*a*b* between the two stimuli across the sampled representative observers, a solid ellipse of $X = [\Delta L* \quad \Delta a* \quad \Delta b*]$ values about the mean satisfying[26]:

$$X^T\Sigma_{\text{Lab}}^{-1}X = X_2^2(\alpha) \tag{19}$$

has probability of $1-\alpha$ for $X_2^2(\alpha)$ the chi-squared distribution having two degrees of freedom. For 95% confidence, $\alpha = 1-0.95 = 0.05$ and $X_2^2(0.05) = 5.99$.

Converting to polar coordinates $X = \Delta C[\sin\gamma\cos\alpha \quad \sin\gamma \sin\alpha\cos\gamma]$ for $\Delta C = \sqrt{(a*)^2+(b*)^2}$ the difference in chroma, Eq. (19) becomes:

$$\begin{aligned}&\Delta C^2[\sin\gamma\ \cos\alpha \quad \sin\gamma\ \sin\alpha \quad \cos\gamma]^T\\ &\Sigma_{Lab}^{-1}[\sin\gamma\ \cos\alpha \quad \sin\gamma\ \sin\alpha \quad \cos\gamma] = 5.99\end{aligned} \tag{20}$$

or:

$$\Delta C = \sqrt{5.99/[\sin\gamma\ \cos\alpha \quad \sin\gamma\ \sin\alpha \quad \cos\gamma]^T\Sigma_{Lab}^{-1}[\sin\gamma\ \cos\alpha \quad \sin\gamma\ \sin\alpha \quad \cos\gamma]} \tag{21}$$

Figure 15 illustrates the resulting estimated ellipse in $\Delta a*$ and $\Delta b*$ for six (6) of the 24 X-Rite Color Checker Chart patches compared with the individual differences for each of the representative population of observers and their 95% confidence ellipse.

It is noted that the 95th percentile ellipse from the population and that from the analysis of variance are in the same order of magnitude, but not exactly equal, simply because the assumption of normality is not strictly held, and there is some correlation across wavelengths and within a single cone response that is also not modeled. Another specific example is that the Monte Carlo analysis sampling of the cone response variability was done in wave-number, not wavelength. Hence, one would not expect it to be normal in wavelength as they are unrelated. Further, the 2000 Census distribution for age is not normal, nor is it even a function of wavelength. Given these shortcomings of the Monte Carlo model and the statistical error propagation model, it is quite remarkable that the simplified prediction of confidence ellipsoids is such an accurate predictor of the individual observer predictions (which require substantially more computational work to obtain).

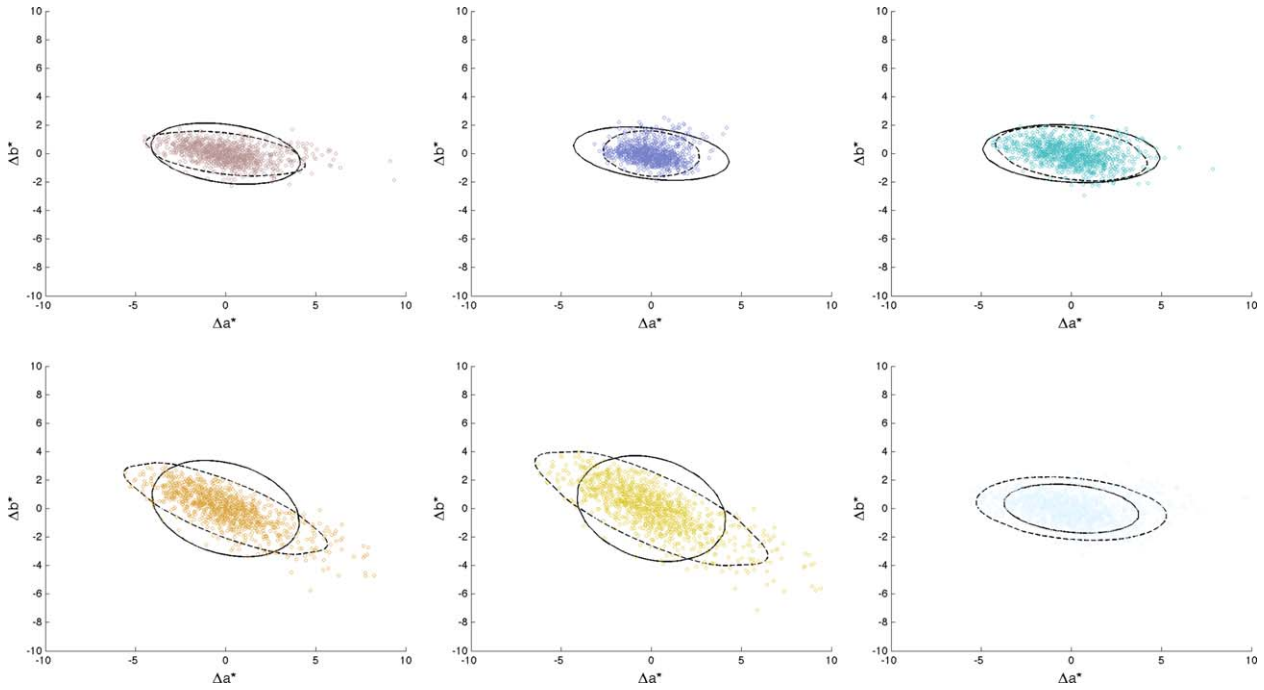

Fig. 15. The variability in the sampled differences, Δa^* and Δb^*, computed from the individual CMFs for each of the population of 1,000 observers (the individual points denoted as "o"), their 95% confidence ellipse (dotted line), and the estimated 95% confidence interval from analysis of variance (solid line) for a selected subset of patches from the X-Rite Color Checker Chart.

SUMMARY AND CONCLUSIONS

Observer metamerism was realistically quantified over a representative population of 1000 human observers using Monte Carlo analysis techniques that sample relatively recent statistical data describing the differences in the factors that affect the spectral response of the human eye. This sample set was then reduced to a complete description that includes its mean LMS cone spectral response functions and their variance and covariance using the analysis of variance procedure suggested by Nimeroff in 1965.[1]

From this description, a procedure is given for expressing an arbitrary set of color matching functions as a linear combination of the mean LMS cone spectral response functions and their variance and covariance. This procedure was then applied to the CIE 1931 and 1964 standard observers thereby providing their respective variance and covariance over a representative population of human observers. These functions can be used, along with the CIE standard observers to predict metameric color matches for the average observers along with 95% confidence ellipsoids on the range of color mismatches for various humans with normal color vision. These ellipsoid ranges (or mismatch gamuts) depend both on the properties of the observers (quantified in this article) and the spectral mismatches of the stimuli in question (the application).

Finally, metametric pairs were rendered from a selected set of patches in the X-Rite Color Checker Chart–one to a broadband CRT display and the other to a narrowband, LED backlit, LCD display. The pairs were rendered to match for the CIE 1931 standard observer. Then, solely from the covariance matrix derived for the CIE 1931 Observer and the differences in the spectra of the pair, a procedure was derived and applied to quantify and draw the 95th percentile ellipsoid in the degree of miss-match in CIE L*a*b* across the representative population. The resulting ellipsoid was shown to be within the same order of magnitude as the computed differences in CIE L*a*b* for each of the 1,000 observers, and a 95th percentile ellipse derived from the covariance matrix for these computed differences. The differences in the ellipsoids were accounted for by noting deviations from normality in the original Monte Carlo analysis sampling process.

These applications demonstrate the utility of the Nimeroff representation that he characterized as a complete representation of the standard observer or any arbitrary observer. From this representation, many other applications are possible. The design of toners for paint, dyes for printing, or the primaries of a color display can now be easily evaluated and perhaps optimized for observer metamerism. Observer metamerism can now be quantified for specification in color standards in terms that are measurable. At last, the system that Nimeroff proposed in 1961 has been fully quantified and accurately implemented for CIE colorimetry. It is perhaps time that the CIE recognized the importance of variance-covariance functions to be paired with mean color matching functions and proposed a new standard for colorimetry that includes both or an extension of the CIE 2006 model for cone fundamentals that includes variance-covariance functions as well.

1. Nimeroff Rosenblatt JR, Dannemiller MC. Variability of spectral tristimulus values. J Res NBS 1961;65:475–483.
2. Berns RS. Billmeyer and Saltzman's Principles of Color Technology, 3rd edition. New York: Wiley; 2000. pp 50–53.
3. CIE Publ. 080-1989: Special Metamerism Index: Observer, Vienna: CIE Central Bureau, 1989.
4. Wyszecki G, Stiles WS. Color Science: Concepts and Methods, Quantitative Data and Formulae, 2nd edition. New York: Wiley; 1982. pp 591–604.
5. Neitz M, Neitz J. Molecular genetics for color vision and color vision defects. Arch Ophthalmol 2000;118:691–700.
6. Merbs SL, Nathans J. Absorption spectra of human cone pigments. Nature 1992;356:433–435.
7. Asenjo AB, Rim J, Oprian DD. Molecular determinants of human red/green color discrimination. Neuron 1994;12:1131–113.
8. Sharpe LT, *et al*. Red, green, and red-green hybrid pigments in the human retina: Correlations between deduced protein sequences and psychophysically measured spectral sensitivities. J Neurosci 1998;18: 10053–10069.
9. Stockman A, Sharpe LT, Fach CC. The spectral sensitivity of the human short- wavelength cones. Vision Res 2000;39:2901–2927.
10. Stockman A, Sharpe LT. Spectral sensitivities of the middle- and long-wavelength sensitive cones derived from measurements in observers of known genotype. Vision Res 2000;40:1711–1737.
11. CIE Publ. 170-1:2006: Fundamental Chromaticity Diagram with Physiological Axes - Part 1. Vienna: CIE Central Bureau, 2006. pp 170–171.
12. Webster MA, MacLeod D. Factors underlying individual color differences in the color matches of normal observers. J Opt Soc Am A 1988; 1722–1735.
13. Viénot, F. What are observers doing when making color matches. De Farbe 1987;34:221–228.
14. Fairchild MD. Modeling Observer Metamerism through Monte Carlo Simulation. OSA Annual Meeting, Rochester; 1996. pp 126.
15. Pokorny J, Smith VC. How much light reaches the retina?. Colour vision deficiencies XIII. Netherlands: Springer, 1997;491–511.
16. Pokorny J, Smith VC, Lutze M. Aging of the human lens. Appl Opt 1987;26:1437–1440.
17. Xu J, Pokorny J, Smith VC. Optical density of the human lens. J Opt Soc Am A 1997;14:953–960.
18. Bone RA, Landrum JT, Cains A. Optical density spectra of the macular pigment in vivo and in vitro. Vision Res 1992;32:105–110.
19. Berendschot TT, van Norren D. Objective determination of the macular pigment optical density using fundus reflectance spectroscopy. Arch Biochem Biophys 2004;430:149–155.
20. Van de Kraats J, Kanis MJ, Genders SW, van Norren D. Lutein and zeaxanthin measured separately in the living human retina with fundus reflectometry. Inv Ophthal Vis Sci 2008;49:5568–5573.
21. Dartnall HJA. The interpretation of spectral sensitivity curves. Brit Med Bull 1953;9:24–30.
22. Govardovskii VI, Fyquist N, Reuter T, Kuzmin G, Donner K. In search of the visual pigment template. Vis Neurosci 2000;17:509–528.
23. Lamb TD. Photoreceptor spectral sensitivities: common shape in the long wavelength region. Vision Res 1951;35:2083–3091.
24. Burns PD, Berns RS. Error propagation analysis in color measurement and imaging. Color Res Appl 1997;22:280–289.
25. Alfvin RL, Fairchild MD. Observer variability in metameric color matches using color reproduction media. Color Res Appl 1997;22:174–188.
26. Johnson RA, Wichern DW. Applied Multivariate Statistical Analysis, 5th edition. Upper Saddle River, NJ: Prentis Hall; 2002. pp 99–100.